Acta Oceanol. Sin., 2018, Vol. 37, No. 11, P. 77–87
DOI: 10.1007/s13131-018-1335-9
http://www.hyxb.org.cn
E-mail: hyxbe@263.net

Analysis of impacting factors on polarimetric SAR oil spill detection

SONG Shasha[1, 2], ZHAO Chaofang[1, 3*], AN Wei[2], LI Xiaofeng[4], WANG Chen[1]

[1] College of Information Science and Engineering, Ocean University of China, Qingdao 266100, China

[2] Post-doctoral Station, China Offshore Environmental Services Ltd., Tianjin 300457, China

[3] Laboratory for Regional Oceanography and Numerical Modeling, Pilot National Laboratory for Marine Science and Technology (Qingdao), Qingdao 266100, China

[4] National Oceanic and Atmospheric Administration, Maryland 20740, USA

Received 8 November 2017; accepted 5 February 2018

Abstract

Polarimetric synthetic aperture radar (SAR) oil spill detection parameters conformity coefficient (μ), Muller matrix parameters ($|C|$, B_0), the eigenvalues of simplified coherency matrix (λ_{nos}) and the influence of SAR observing parameters, ocean environment and noise level are investigated. Radarsat-2 data are used to make systematic analysis of polarimetric parameters for different incidences, wind speeds, noise levels and the ocean phenomena (oil slick and look likes). The influence of the SAR observing parameters, the ocean environment and the noise level on the typical polarimetric SAR parameter conformity coefficient has been analyzed. The results indicate that conformity coefficient cannot be simply used for oil spill detection, which represents the image signal to the noise level to some extent. When the signals are below the noise level for the oil slick and the look likes, the conformity coefficients are negative; while the signals above the noise level corresponds to positive conformity coefficients. For dark patches (low wind and biogenic slick) with the signal below the noise, polarization features such as conformity coefficient cannot separate them with oil slick. For the signal above the noise, the oil slick, the look likes (low wind and biogenic slick) and clean sea all have positive conformity coefficients, among which, the oil slick has the smallest conformity coefficient, the look likes the second, and the clean sea the largest value. For polarimetric SAR data oil spill detection, the noise plays a significant role. So the polarimetric SAR data oil spill detection should be carried out on the basis of noise consideration.

Key words: multi-polarimetric SAR, oil spill, conformity coefficient, noise

Citation: Song Shasha, Zhao Chaofang, An Wei, Li Xiaofeng, Wang Chen. 2018. Analysis of impacting factors on polarimetric SAR oil spill detection. Acta Oceanologica Sinica, 37(11): 77–87, doi: 10.1007/s13131-018-1335-9

1 Introduction

The development of satellite remote sensing technology has brought up more and more polarimetric SAR data to us, from the SIR-C of US space shuttle, Radarsat-2, TerraSAR, ALOS PALSAR, UARSAR, China GF-3 and so on. The investigation of the polarimetric SAR data for oil spill monitoring has been carried out widely. Proposed polarimetric SAR oil spill detection methods include coherent matrix eigen composition, Muller matrix parameters, co-polarized phase difference standard deviation, and the conformity coefficient and so on (Nunziata et al., 2008, 2015; Migliaccio et al., 2009, 2011, 2012; Zhang et al., 2011; Liu et al., 2011; Li et al., 2013, 2017; Buono et al., 2016; Song et al., 2017). There is a promising application for the polarimetric SAR data oil spill detection.

Although many methods for the polarimetric SAR oil spill detection have been proposed, the determination criteria of oil slick, free surface and look likes under different observing conditions and ocean environment are inconsistent. Especially, there is the lack of systematic analysis of the noise influence on the polarimetric SAR oil slick detection. The currently used polarimetric SAR data are featured with different noise levels, depending on antenna patterns, remitting power and receiver noise (Velotto et al., 2011). For example, the different modes of TerraSAR-X have the noises between –19 and –26 dB, an averaged noise for ALOS PALSAR –30 dB, Radarsat–2 (–36.5±3) dB, C band of SIR-C/X SAR –28 dB and UAVSAR –35 to –53 dB (Nunziata et al., 2012, 2013; Minchew et al., 2012). Velotto Domenico et al. (2011) used two polarized TerraSAR-X images to analyze the influence of the noise on co-polarization phase difference, and pointed out that most low SNR pixels came from oil. Minchew Brent used the polarimetric SAR data for deep water horizon oil spill analysis and proposed that additive noise could be featured using the fourth eigenvalue of T4 matrix. Skrunes Stine et al. (2014) compared NRCS (normalized radar cross section) and NESZ (noise equivalent sigma zero) of co-polarization and cross-polarization channels of the clean sea surface, plant oil, emulsified oil and crude oil using two Radarsat–2 images acquired with different incidences in Norwegian oil-on-water exercise in June 2011. The result shows that cross-polarization is significantly influenced by noises with averaged SNR –2 dB, so co-polarization is chosen for polarization parameters extraction and oil detection. The co-polarization data could reduce the impacts of the noise to some extent, but the noise still could not be ignored at all. Additionally, the co-polarization coherency matrix could not make full use of

Foundation item: The Shandong Natural Science Joint Foundation of China under contract No. U1606405.
*Corresponding author, E-mail: zhaocf@ouc.edu.cn

the advantages of quad-polarization. Generally speaking, the systematic analysis of the influence of observing condition, environment parameters and the noise level on the polarization parameters has not been done for oil spill identification. Meanwhile, the simultaneous consideration of observing conditions, environment parameters and image noises has not been carried out for polSAR oil spill detection.

The paper collects Radarsat-2 polarization data of different incidences, wind speeds, noise levels and surface phenomena (oil and look likes) to analyze the impacts of the observing conditions, the environment parameters and the noise levels on the polarization parameters of the oil spill detection. The paper concludes the following sections. Section 1 is a brief introduction. Section 2 describes the data used in the paper. Section 3 introduces three polarimetric parameters, and Section 4 makes the analysis of the three parameters and the influence of the observing conditions, the environmental parameters and the image noises on the polarization parameters. The verification is also included. Finally, a conclusion is given in Section 5.

2 SAR data

Eight Radarsat-2 images of the China offshore, the Gulf of Mexico and the North Sea from 2008 to 2012 have been used. The phenomena in SAR images include oil slick, low wind area and biogenic slicks. The images cover incidence 29°–50°, NESZ –31 to –36 dB, and wind speed 1.6–9.0 m/s, as shown in Table 1. The incidence angle and the NESZ are acquired from head file, where the incidence increases with the beam number, and the NESZ increases with incidence. The wind speed is obtained from literature and NCEP forecast wind. Two typical SAR images are used in Section 4.1 to investigate the three polarimetric parameters mentioned in Section 3, and all of the eight images are used in Section 4.1 to analyze the influence of the observing conditions, the environmental parameters and the image noises on the polarization parameters.

Table 1. Polarization SAR data

No.	UTC time	Location	Mode	NESZ/dB	Incidence/(°)	Wind speed/m·s^{-1}	Dark phenomena
1	2010-05-15 11:56	28.5°N, 88.3°W	FQ10	–33.3 to –35.6	29.2–30.9	9.0	oil slick
2	2011-06-08 17:27	60.0°N, 2.3°E	FQ15	–33.0 to –35.0	34.5–36.1	1.6–3.3	oil slick
3	2008-07-13 10:49	18.2°N, 109.8°E	FQ15	–33.1 to –35.8	34.4–36.0	2.0–3.0	low wind area
4	2012-08-18 22:12	20.7°N, 116.7°E	FQ10	–33.1 to –35.7	29.2–30.9	2.0–2.3	low wind area
5	2011-05-16 10:09	38.3°N, 118.8°E	FQ25	–31.5 to –32.8	43.6–44.9	2.0–3.0	low wind area
6	2010-05-08 12:01	26.8°N, 92.0°W	FQ23	–32.0 to –33.0	41.9–43.3	6.5	oil slick
7	2012-08-13 22:57	20.7°N, 116.6°E	FQ31	–31.3 to –32.1	48.3–49.5	3.0–5.0	biogenic slick
8	2008-08-23 10:53	18.2°N, 109.6°E	FQ21	–32.1 to –34.2	40.1–41.6	3.0	low wind area

3 Polarimetric parameters

The paper lays emphasis on the polarization SAR parameters representing the relative magnitudes of co-polarization and cross-polarization powers, including the conformity coefficient (μ), the Muller parameters ($|C|$, B_0) and the eigenvalues (λ_{nos}) of the simplified coherency matrix.

3.1 *Conformity coefficient*

The concept of the conformity coefficient originates from the inversion of soil moisture from compact polarimetry data (Dubois-Fernandez et al., 2008). The parameter can discriminate surface scattering, double-bounce scattering and volume scattering. The conformity coefficient is expressed as

$$\mu \approx \frac{2\left[Re\left(S_{HH}S_{VV}^{*}\right)-\left|S_{HV}\right|^{2}\right]}{\left(\left|S_{HH}\right|^{2}+2\left|S_{HV}\right|^{2}+\left|S_{VV}\right|^{2}\right)}, \tag{1}$$

where S_{HH}, S_{HV} and S_{VV} are the complex amplitudes of the scattering matrix, subscripts H and V represents remitting and receiving polarization.

For land surfaces, S_{HV} is small, S_{HH} and S_{VV} are relevant, phase difference is close to 0, so conformity coefficient is positive, $t_1<\mu<1$, where t_1 is a threshold value larger than 0.

For double-bounce scattering targets, S_{HH} and S_{VV} are relevant, phase difference is close to 180°, so conformity coefficient is negative, $-1<\mu<t_2$, where t_2 is threshold value below 0.

For volume scattering, S_{HH} and S_{VV} are weakly correlated, S_{HV} is large, so $t_1<\mu<t_2$, t_1, t_2 are determined by statistics.

When the sea surface is well modeled by Bragg scattering (Schuler et al., 1993; Zhang et al., 2011), S_{HV} is small, close to 0, and S_{HH} and S_{VV} are highly correlated with phase difference close to 0, so $\mu>0$; when it is non-Bragg scattering, vessels for example, S_{HH} and S_{VV} are weakly correlated with phase difference close to 180°, so $\mu<0$.

3.2 *Muller parameters*

Muller matrix gives the relationship between an incident Stokes vector and a reflecting Stokes vector (Van Zyl et al., 1987; Guissard, 1994), which could be expressed by a 4×4 matrix:

$$\left\langle \vec{g^{s}} \right\rangle = \langle M \rangle \vec{g^{i}}, \tag{2}$$

where $\vec{g^{i}}$ and $\vec{g^{s}}$ are the incident Stokes vector and the reflecting Stokes vector, respectively.

For the sea surface, there are only eight non-zero elements in the Muller matrix, considering the low correlation between co- and cross-polarization (Cloud, 1985; Van Zyl, 1989; Nghiem et al., 1992; Ulaby et al., 1992),

$$M=\begin{pmatrix} A+B_0 & B & 0 & 0 \\ B & A-B_0 & 0 & 0 \\ 0 & 0 & C+B_0 & D \\ 0 & 0 & -D & C-B_0 \end{pmatrix}, \tag{3}$$

where

$$A=\frac{1}{2}\left\langle \left|S_{HH}\right|^{2}+\left|S_{VV}\right|^{2}\right\rangle, \tag{4}$$

$$B=\frac{1}{2}\left\langle \left|S_{HH}\right|^{2}-\left|S_{VV}\right|^{2}\right\rangle, \tag{5}$$

$$B_0 = \left\langle |S_{HV}|^2 \right\rangle, \tag{6}$$

$$C = \langle \Re (S_{HH} S_{VV}^*) \rangle, \tag{7}$$

$$D = \langle \Im (S_{HH} S_{VV}^*) \rangle. \tag{8}$$

$|C|$ is related to S_{HH} and S_{VV}, and B_0 are related to S_{HV}. For the clean sea, Bragg scattering is dominated for sea surface, S_{HH} and S_{VV} are highly correlated, S_{HV} is small, so $|C|>B_0$ (Nunziata et al., 2008). For the oil slick, S_{HH} and S_{VV} are weakly correlated, so $|C|<B_0$ (Nunziata et al., 2008).

3.3 *Eigenvalues of simplified coherency matrix*

For natural medium, such as soil and forest, the correlation between the co-polarization and the cross-polarization is nearly 0 under the reflecting symmetry hypothesis (Nghiem et al., 1992; Allain et al., 2005; Wang et al., 2015).

The scattering matrix based on Pauli basis is expressed as

$$\boldsymbol{k} = \begin{bmatrix} S_{HH} + S_{VV} & S_{HH} - S_{VV} & 2S_{HV} \end{bmatrix}. \tag{9}$$

The coherency matrix of polarization SAR data is

$$\boldsymbol{T} = \boldsymbol{k} * \boldsymbol{k}_T^* = \frac{1}{2} \begin{bmatrix} |x_1|^2 & x_1 x_2^* & 2x_1 S_{HV}^* \\ x_2 x_1^* & |x_2|^2 & 2x_2 S_{HV}^* \\ 2S_{HV} x_1^* & 2S_{HV} x_2^* & 4|S_{HV}|^2 \end{bmatrix}, \tag{10}$$

where x_1=S_{HH}+S_{VV}, x_2=S_{HH}-S_{VV}.

The simplified coherency matrix considering the reflecting symmetry hypothesis is

$$\boldsymbol{T} = \frac{1}{2} \begin{bmatrix} |x_1|^2 & x_1 x_2^* & 0 \\ x_2 x_1^* & |x_2|^2 & 0 \\ 0 & 0 & 4|S_{HV}|^2 \end{bmatrix}. \tag{11}$$

The eigenvalue could be acquired by Eigen decomposition (Guissard, 1994):

$$\lambda_{1,\,nos} = \frac{1}{2} \left\{ x_3 + \sqrt{(x_4)^2 + 4 \left\langle |S_{HH} S_{VV}^*|^2 \right\rangle} \right\}, \tag{12}$$

$$\lambda_{2,\,nos} = \frac{1}{2} \left\{ x_3 - \sqrt{(x_4)^2 + 4 \left\langle |S_{HH} S_{VV}^*|^2 \right\rangle} \right\}, \tag{13}$$

$$\lambda_{3,\,nos} = 2 \left\langle |S_{HV}|^2 \right\rangle, \tag{14}$$

where $x_3 = \left\langle |S_{HH}|^2 \right\rangle + \left\langle |S_{VV}|^2 \right\rangle$, $x_4 = \left\langle |S_{HH}|^2 \right\rangle - \left\langle |S_{VV}|^2 \right\rangle$. The first and second eigenvalues of the simplified coherency matrix are related to co-polarization backscatter and correlation coefficient, and the third one is related to the multi-scattering of rough surfaces corresponding to the cross-polarization channel. For the clean sea, $\lambda_{1,\,nos}>\lambda_{3,\,nos}$ due to the low cross-polarization intensity; for the oil slick, the expression of $\lambda_{1,\,nos}$ is too complex to give direct answer which one is larger for $\lambda_{1,\,nos}$ and $\lambda_{3,\,nos}$. A detailed analysis would be carried out in the following experiments.

4 Data analysis

4.1 *Analysis of three polarization parameters*

The eight Radarsat-2 SAR images are divided into two groups. Group 1 includes No. 1 to No. 4 images in Table 1, with an incidence range of 30°–36° and the NESZ of –33 to –36 dB. The fifth to eighth images are Group 2 with an incidence range of 40°–50° and the NESZ of –31 to –34 dB. First, one typical SAR image is chosen from each group respectively for analysis. The SAR image acquired on May 15, 2010 from the Gulf of Mexico is chosen from Group 1, and a SAR image of the Gulf of Mexico on May 8, 2010 is chosen from Group 2, as shown in Fig. 1. The dark patches in Fig. 1a are oil slicks with an image incidence angle of 29°– 31° and the wind speed of 9 m/s. The dark patches in Fig. 1b are also oil slicks, with an incidence angle of 42°–45° and the wind speed of 6.5 m/s (Li et al., 2013).

To analyze the noise level of the two images, the signal-noise-ratio (SNR, r_{sn}) probability density function (pdf) is plotted in Fig. 2, where the full line stands for the oil slick and dashed line for the clean sea. SNR is calculated by r_{sn}=σ^0–n_a, where σ^0 is the backscattering intensity and n_a the averaged NESZ. The noise level of the two images are –33.3 to –35.6 and –32 to –33 dB respectively. The co-polarization channel of the SAR data in the Fig. 1a has a large backscatter intensity, and the averaged VV backscatter intensity of the oil slick is –24 dB and the clean sea –15 dB, so the corresponding averaged signal of the clean sea and oil slick in Fig. 2a is above the noise level. The backscatter intensity of the oil area in Fig. 1b is weak and the corresponding averaged signal of oil in Fig. 2b is below the noise level.

At first we compare the conformity parameters of the oil slick and the clean sea in the two typical SAR images. The conformity coefficient is analyzed combined with co-polarization phase difference as shown in Fig. 3. Figure 3a gives the co-polarization phase difference pdf of the SAR data on May 15, where the clean sea has smaller standard deviation than the oil slick. The corresponding conformity coefficient is larger than that of oil (Fig. 3c). Please note that both the clean sea and the oil slick have the positive conformity coefficient, indicating that conformity coefficient cannot be simply used for the discrimination of the oil slick and the clean sea. The positive or negative conformity coefficient does not absolutely indicate the clean sea or oil slick. The case of the SAR data on May 8 is given in Figs 3b and d, where the co-polarizations are highly correlated for the clean sea area with a narrow pdf and the co-polarization phase difference pdf of oil is nearly uniform distribution, indicating the co-polarizations are uncorrelated for oil. The corresponding conformity coefficient of oil is negative and the clean sea positive (Fig. 3d). Considering the incidence angle of the two images, for a medium incidence angle (≈30°), the averaged SNR of oil is above 0, and the conformity coefficient is positive; for a large incidence angle (⩾40°), the averaged SNR of oil is below 0, and the conformity coefficient is positive. The wind speeds of the two images are medium to high speeds (6–9 m/s). The case of low wind will be discussed later.

Next, we compare the Muller matrix parameters ($|C|$, B_0) and eigenvalues of simplified coherency matrix ($\lambda_{1,\,nos}$, $\lambda_{3,\,nos}$). The $|C|$, B_0 parameters of the oil slick and the clean sea in SAR data on May 15 and May 8, 2010 are given in Fig. 4, with the full line for oil, the dashed line for clean sea, thin line for $|C|$, bold line for B_0. $|C|$ is related to the co-polarization and B_0 is related to the cross-polarization. Both oil and clean sea satisfy $|C|>B_0$ and positive

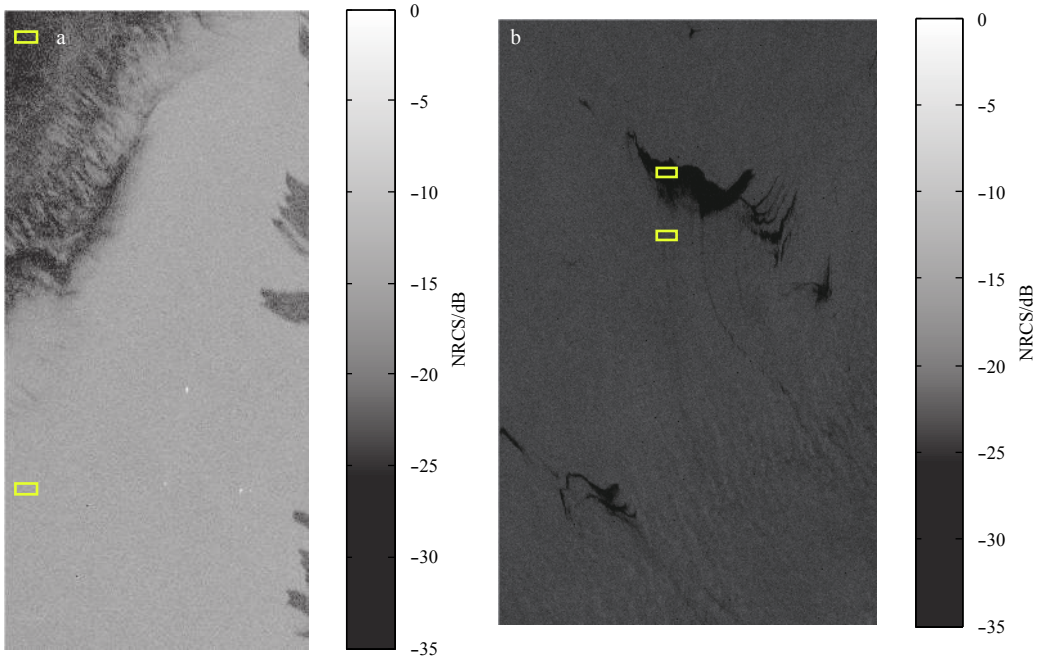

Fig. 1. VV polarization images of the SAR data acquired on May 15 and May 8, 2010.

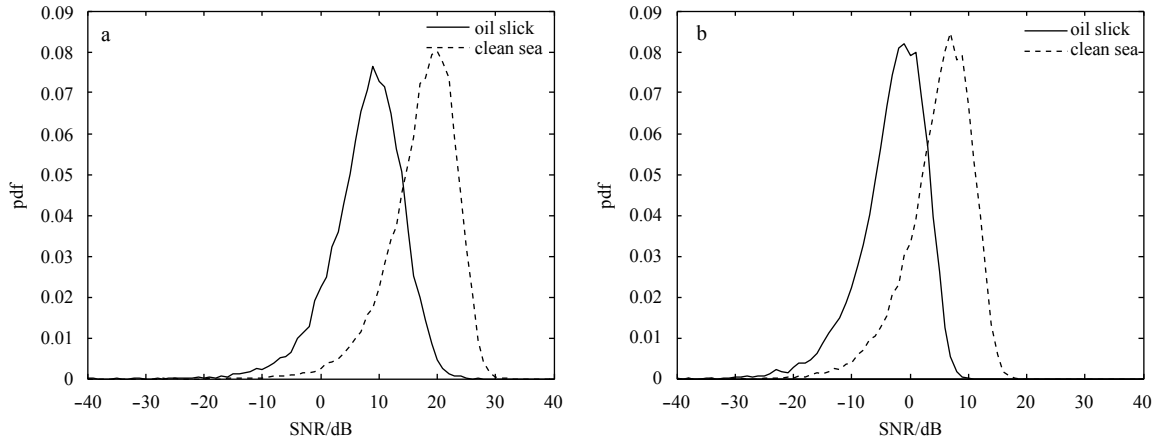

Fig. 2. The VV polarization SNR pdf of the oil slick (full line) and the clean sea (dashed line) of the SAR data: the image on May 15, 2010 (a) and the image on May 8, 2010 (b).

$|C|$–B_0 in the SAR data on May 15, 2010. The clean sea has the positive value for $|C|$–B_0, while the oil slick has negative $|C|$–B_0 in May 8, 2010 data. Large difference between the oil slick and the clean sea is found in $|C|$ parameter; while B_0 for the oil slick and the clean sea is nearly the same. Figure 5 compares the eigenvalues of simplified coherency matrix, where the thin line stands for $\lambda_{1,\,nos}$, the bold line for $\lambda_{3,\,nos}$, the full line for oil, and the dashed line for clean sea. For the SAR data on May 15, 2010, both oil and clean sea satisfy $\lambda_{1,\,nos}>\lambda_{3,\,nos}$ and positive $\lambda_{1,\,nos}-\lambda_{3,\,nos}$; for the data on May 8, 2010, the clean sea satisfies $\lambda_{1,\,nos}>\lambda_{3,\,nos}$ and positive value for $\lambda_{1,\,nos}-\lambda_{3,\,nos}$, while for the oil slick, $\lambda_{1,\,nos}$ and $\lambda_{3,\,nos}$ are almost the same.

The comparison of the three polarization SAR parameters shows that they have consistent performance in the same images. For oil slick and clean sea samples, when conformity coefficient is positive, Muller matrix parameters $|C|>B_0$ and eigenvalues of simplified coherent matrix $\lambda_{1,\,nos}>\lambda_{3,\,nos}$; when conformity coefficient is negative, $|C|<B_0$ and $\lambda_{1,\,nos}$, $\lambda_{3,\,nos}$ are nearly the same. The formulations of the parameters in Section 3 also indicate the same characterization of the relative magnitude of co-polarization and cross-polarization. Consequently, conformity coefficient has been chosen as a typical parameter to analyze the influence of observing conditions, environmental parameters and image noises in detail.

4.2 *Influence of observing conditions, environmental parameters and image noises on polarization parameters*

The influence of the observing conditions, the environmental parameters and the image noises on polarization parameters has been analyzed. In addition to the two images in Section 4.1, another six images are also used as shown in Fig. 6, where the oil slick, clean sea and look likes samples are labeled. Figure 6a is the image acquired during 2011 Norwegian oil-on-water exercise, and the dark patches from the left to the right are plant oil, emulsion and crude oil (chosen for analysis), with a wind speed of 1.6–3.3 m/s (Migliaccio et al., 2011). Figure 6b is a South China

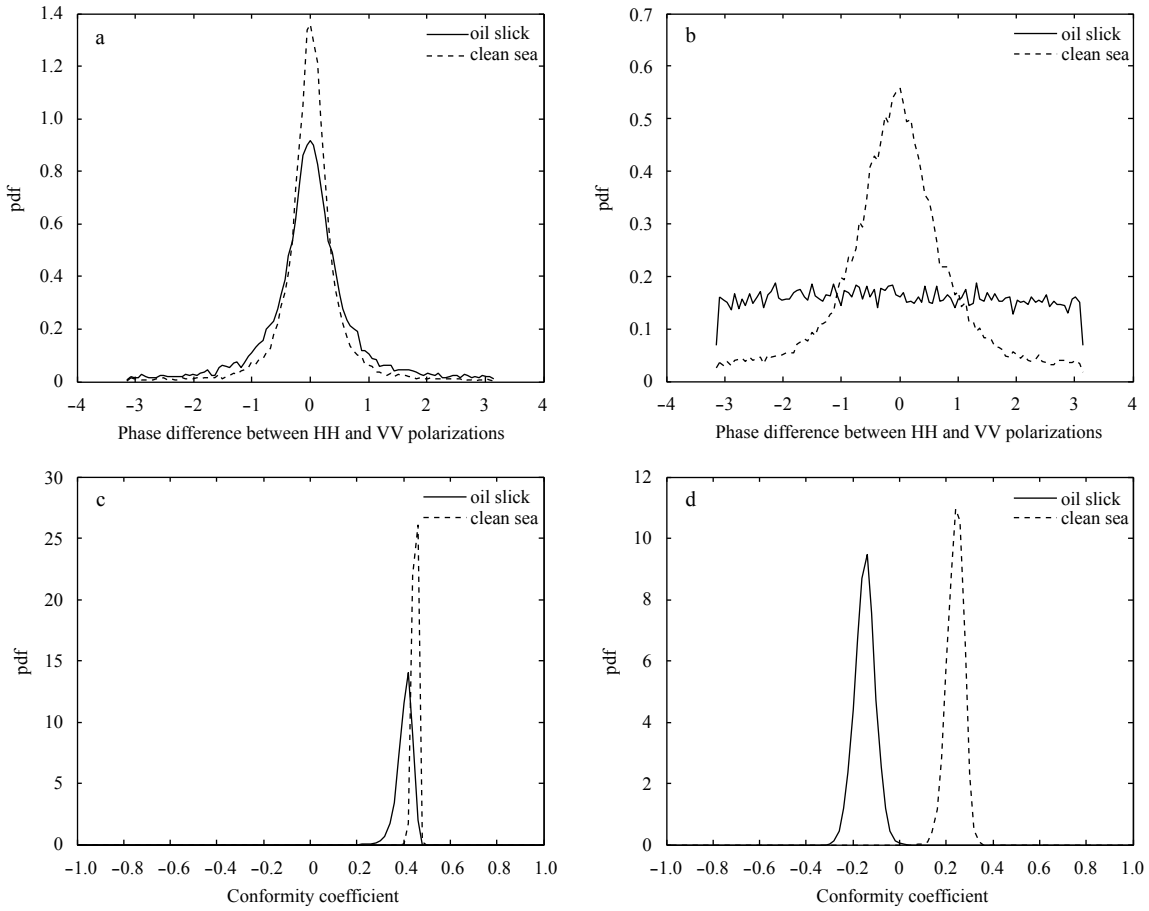

Fig. 3. Co-polarization phase difference and conformity coefficient of oil slick and clean sea for SAR data on May 15 and May 8, 2010. 2010-05-15 co-polarization phase difference pdf (a), 2010-05-08 co-polarization phase difference pdf (b), 2010-05-15 conformity coefficient pdf (c) and 2010-05-08 conformity coefficient pdf (d).

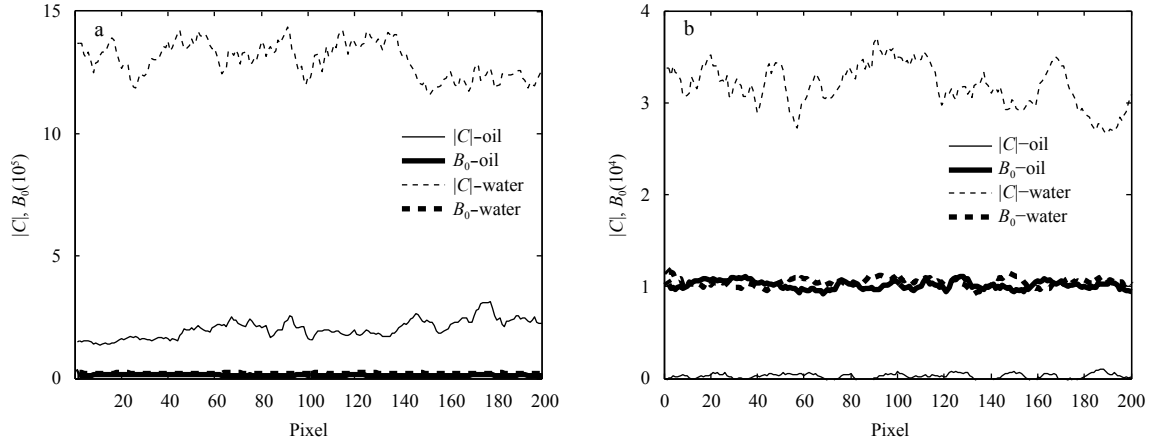

Fig. 4. Muller matrix parameters of polarization SAR data on May 15 and May 8, 2010: $|C|$ and B_0 of SAR data on May 15, 2010 (a) and $|C|$ and B_0 of SAR data on May 8, 2010 (b).

Sea image on July 13, 2008, where the internal waves and the low wind area are clearly visible and the wind speed is 2.0–3.0 m/s according to the NCEP forecast wind. Figure 6c is another South China Sea image on August 18, 2012, also with the internal waves and the low wind area clearly visible, and wind speed of 2.0–2.3 m/s from the NCEP data. The incidence angles of the above three images range from 29° to 36°, with a noise level of –33 to –36 dB. Figure 6d shows a South China Sea image on August 13, 2012, where the dark patches are biogenic slicks and the wind speed is 3.0–5.0 m/s from the NCEP data. Figure 6e is a Bohai Sea image on May 16, 2011, where the left bottom is the look alikes, with a wind speed of 3.0–5.0 m/s from the NCEP data. Figure 6f gives the SAR image of South China Sea on August 23, 2008, where the internal waves are visible and the wind speed is 3.0 m/s from the

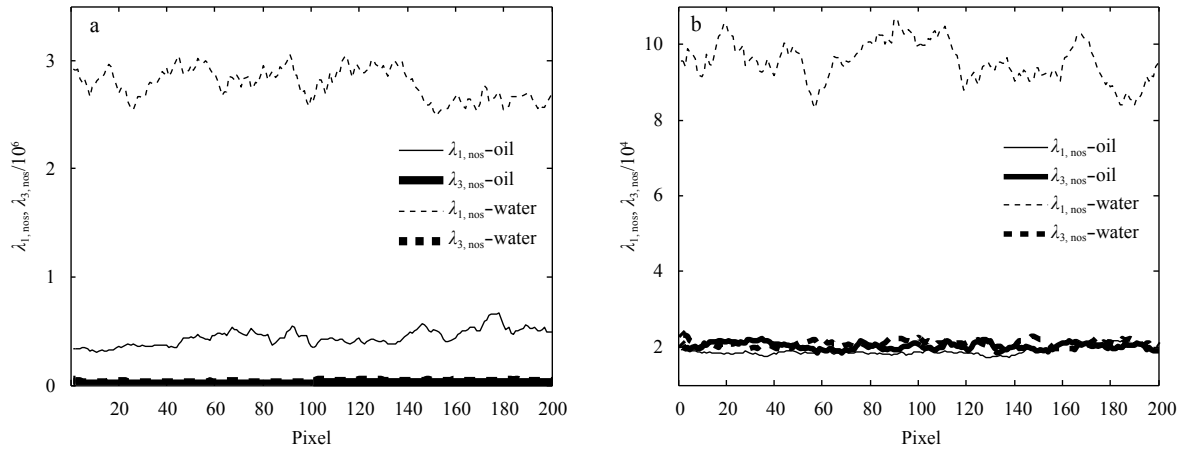

Fig. 5. Eigenvalue $\lambda_{1,\,nos}$ and $\lambda_{3,\,nos}$ of simplified coherency matrix of SAR data on May 15 and May 8, 2010: eigenvalue of simplified coherency matrix of SAR data on May 15, 2010 (a) and eigen value of simplified coherency matrix of SAR data on May 8, 2010 (b).

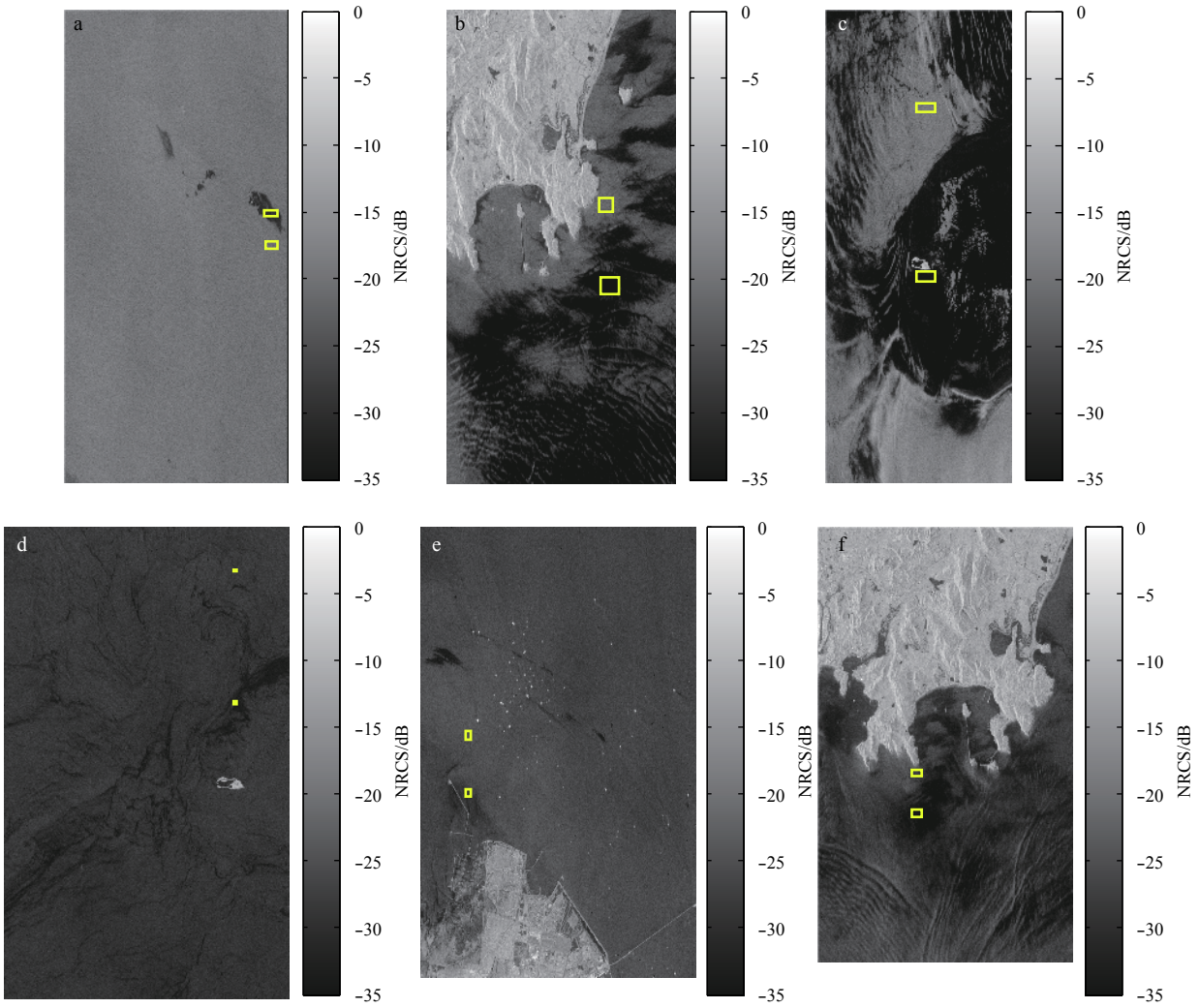

Fig. 6. Another six Radarsat-2 images used for analysis. The image on June 8, 2011 (a), the image on July 13, 2008 (b), the image on August 18, 2012 (c), the image on August 13, 2012 (d), the image on May 16, 2011 (e) and the image on August 23, 2008 (f).

NCEP data. The incidence angles of the three images are 40°–50° and the noise level is –31 to –34 dB.

For the purpose of identifying the relationship between the conformity coefficient and the SAR observing conditions, the environmental parameters and the noise levels, VV polarization SNR, the co-polarization phase and the conformity coefficient pdfs are plotted in Figs 7–12. The VV polarization SNR pdf characterizes the signal and noise of the oil slick, look likes and clean

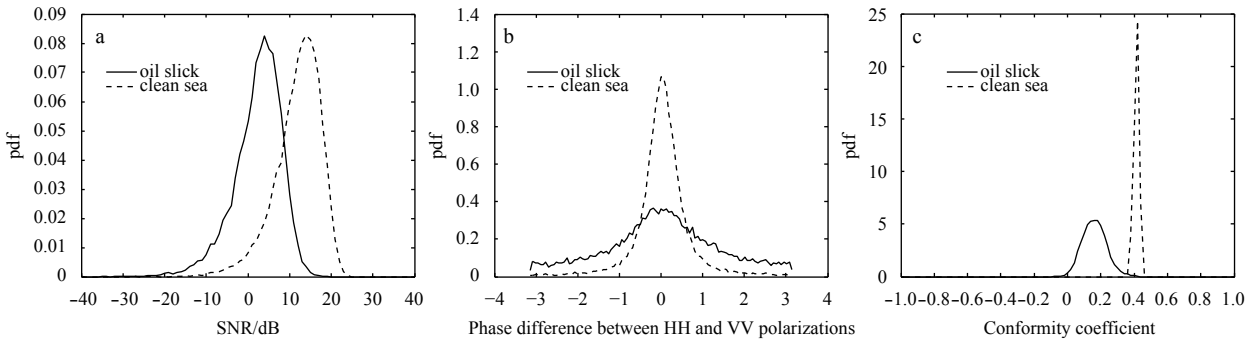

Fig. 7. Polarization parameter pdfs of oil slick and clean sea of Radarsat-2 data on June 8, 2011 (full line for oil slick, dashed line for clean sea). SNR pdf (a), co-polarization phase difference pdf (b) and conformity coefficient pdf (c).

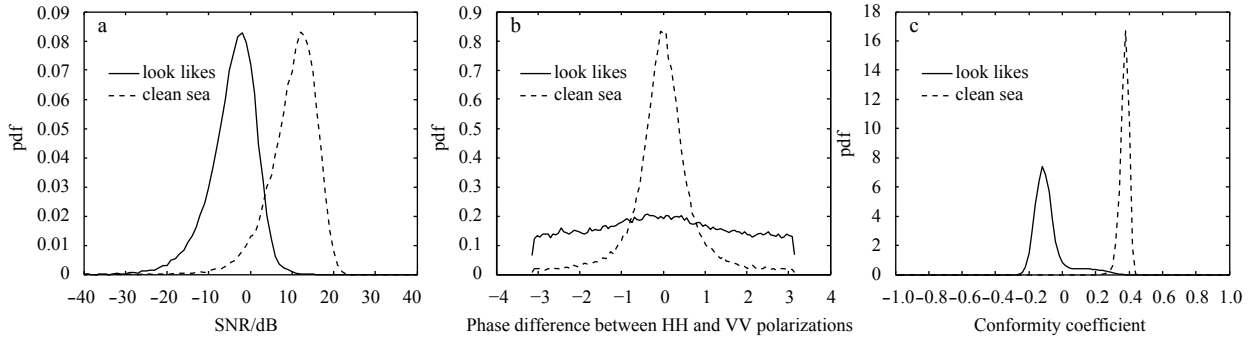

Fig. 8. Polarization parameter pdfs of look likes and clean sea of Radarsat-2 data on July 13, 2008 (full line for look likes, dashed line for clean sea). SNR pdf (a), co-polarization phase difference pdf (b) and conformity coefficient pdf (c).

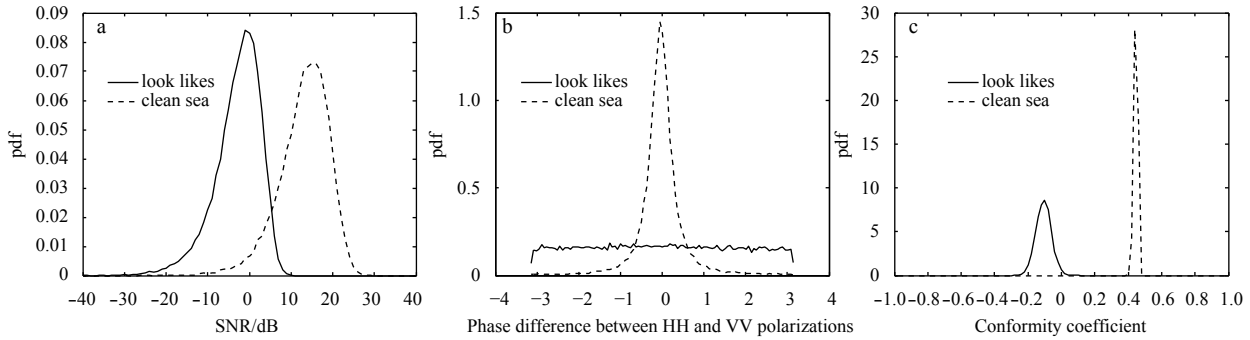

Fig. 9. Polarization parameter pdfs of look likes and clean sea of Radarsat-2 data on August 18, 2012 (full line for look likes, dashed line for clean sea). SNR pdf (a), co-polarization phase difference pdf (b) and conformity coefficient pdf (c).

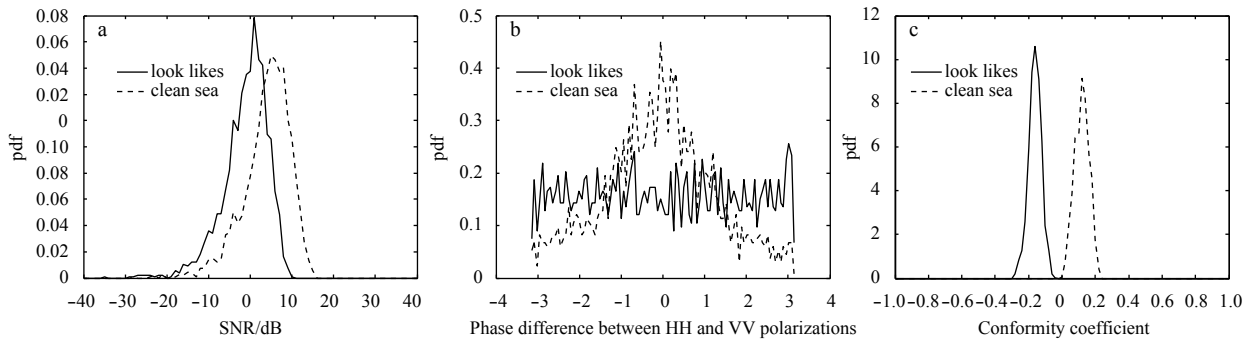

Fig. 10. Polarization parameter pdfs of look likes and clean sea of Radarsat-2 data on August 13, 2012(full line for look likes, dashed line for clean sea). SNR pdf (a), co-polarization phase difference pdf (b) and conformity coefficient pdf (c).

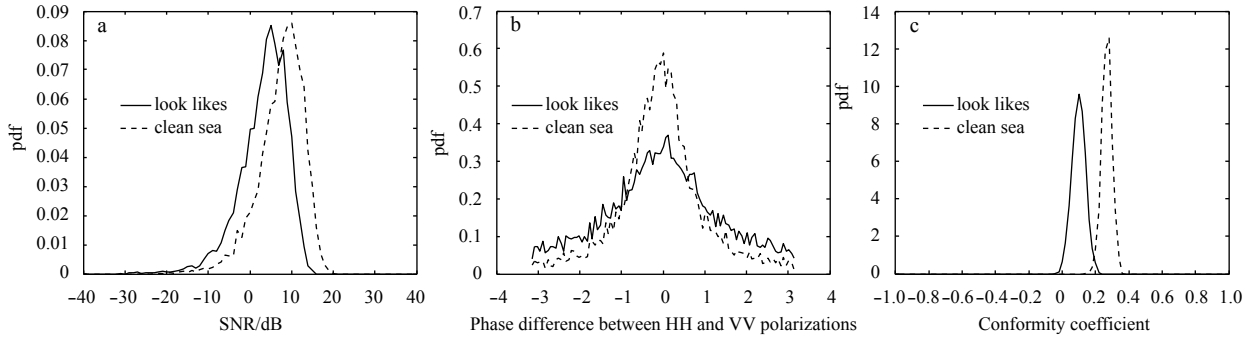

Fig. 11. Polarization parameter pdfs of look likes and clean sea of Radarsat-2 data on May 16, 2011 (full line for look likes, dashed line for clean sea). SNR pdf (a), co-polarization phase difference pdf (b) and conformity coefficient pdf (c).

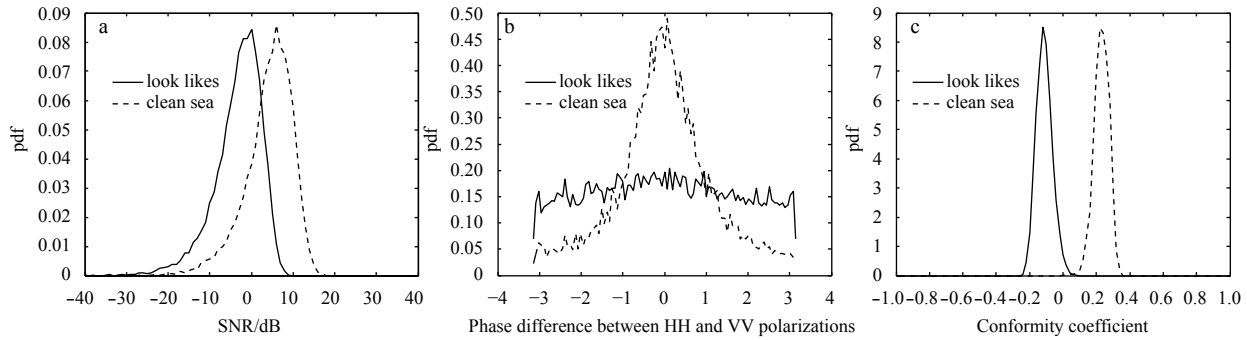

Fig. 12. Polarization parameter pdfs of look likes and clean sea of Radarsat-2 data on August 23, 2008 (full line for look likes, dashed line for clean sea). SNR pdf (a), co-polarization phase difference pdf (b) and conformity coefficient pdf (c).

sea in the SAR data. The co-polarization phase is generally not uniformly distributed. The nearly uniform distribution for the oil slick and the look likes is related to the low SNR and the influence of the noise. The conformity coefficient pdf gives the distribution of the conformity coefficient for the oil slick, the look likes and the clean sea, representing the co-polarization and cross-polarization powers. Note that the vessels and drilling rigs are not included in the analysis for their strong cross-polarization, weak co-polarization and negative conformity coefficient. The clean sea samples in Figs 7–12 all have the signals above the noise, the narrow co-polarization phase difference pdfs and the positive conformity coefficients smaller than 0.5. The oil slick samples of Fig. 7 in the image on June 8, 2011 with an averaged signal above the noise have a broad instead of uniformly distributed phase difference pdf and the positive conformity coefficients, about 0.2 on average. The oil slicks of Fig. 3 in the image on May 15, 2010 also have the signal above noise and the positive conformity coefficient about 0.4. While the oil slicks on May 8, 2010 have the signal below the noise and the negative conformity coefficient about –0.2. The look likes dark patches (low wind and biogenic slicks) in Figs 8–10 and 12 have the signal below the noise, the nearly uniformly distributed phase difference and the negative conformity coefficient about –0.1 on average. While the look likes dark patches in Fig. 11 have the signal above the noise, a broad but not nearly uniformly distributed phase difference pdf and the positive conformity coefficient about 0.1 on average. In summary, the conformity coefficients are positive for the oil slick (the images on May 15, 2010 and June 8, 2011), the clean sea (all the 8 images) and the look likes (the image on May 16, 2011). Conformity coefficients are negative for oil slick (May 8, 2010) and other look likes (July 13, 2008 for example).

In order to discuss the influence of the observing conditions, the environmental parameters and the noises on the conformity coefficient, we summarize the above analysis results in Table 2. It can be seen that dark phenomena (oil slick and low wind area) in the SAR images can also have the positive conformity coefficient,

Table 2. Summary of analysis results

No.	Date	Incidence angle/(°)	Wind speed/m·s^{-1}	Conformity coefficient		Averaged SNR/dB	
				Dark patch	Clean sea	Dark patch	Clean sea
1	2010–05–15	29.2–30.9	9.0	oil slick μ>0	μ>0	r_{sn}>0	r_{sn}>0
2	2011–06–08	34.5–36.1	1.6–3.3*	oil slick μ>0	μ>0	r_{sn}>0	r_{sn}>0
3	2008–07–13	34.4–36.0	2.0–3.0	low wind μ<0	μ>0	r_{sn}<0	r_{sn}>0
4	2012–08–18	29.2–30.9	2.0–2.3	low wind μ<0	μ>0	r_{sn}<0	r_{sn}>0
5	2011–05–16	43.6–44.9	2.0–3.0	low wind μ>0	μ>0	r_{sn}>0	r_{sn}>0
6	2010–05–08	41.9–43.3	6.5	oil slick μ<0	μ>0	r_{sn}<0	r_{sn}>0
7	2012–08–13	48.3–49.5	3.0–5.0	biogenic slick μ<0	μ>0	r_{sn}<0	r_{sn}>0
8	2008–08–23	40.1–41.6	3.0	low wind μ<0	μ>0	r_{sn}<0	r_{sn}>0

such as the oil slick in the images on May 15, 2010 and June 8, 2011, as well as low wind area in the image on May 16, 2011. This indicates that the positive and negative values conformity coefficients are not absolutely corresponding to the oil slick. The images cover a wind range of 2.0–9.0 m/s, from low to high speed, with an incidence angle of 29°–50°, from the medium to large incidences, excluding the impacts of wind and incidence on the conformity coefficient.

The changes of the conformity coefficient are analyzed considering the noise level. It can be seen that the negative conformity coefficient corresponds to an averaged SNR below 0 (averaged signal lower than noise), and the positive conformity coefficient corresponds to high SNR above 0 (averaged signal higher than noise). So it could be concluded to some extent that the positive and negative values of the conformity coefficient measure the image SNR other than discriminating the oil slick and the clean sea. Note that, here we are not trying to confuse the polarimetric properties with scattered power. From the comparison between the conformity coefficient and the SNR, we would like to emphasize that the effectiveness of polarimetric parameters is closely related to the quality of the signals received. For the signals below the noise level, all useful information including polarimetric information is contaminated by noise. So the application of polarimeric parameters should take the noise analysis into account. Otherwise, no stable or convictive conclusions could be achieved.

Next, we continue to analyze the influence of the incidence angle on the conformity coefficient. Nos 1 to 4 images in Table 2 have the medium incidence angle (30°–40°), and the two images of them have the positive SNR for dark area, as well as the positive conformity coefficient. No. 5 to 8 images have the larger incidence angle (40°–50°), and only one image has the positive SNR for the dark area, as well as the positive conformity coefficient, and the other three images have the negative SNR (dB) and the conformity coefficient for the dark area. For the medium incidence angle, SAR has strong backscattering and large SNR, so there is a large probability for the positive SNR. While for the large incidence angle, SAR has weak backscattering, low SNR and a large probability of the negative SNR.

Then, the relationship between the environmental wind parameter and the conformity coefficient has been discussed. No. 1 and 6 images have medium to high wind speed (6.5 and 9.0 m/s), while the other six images have low wind speed (2.0–5.0 m/s), and two images of them have positive conformity coefficient, four images with the negative values for the dark patches, indicating that the conformity coefficient is more probably to be negative under the low wind speed. SAR data have the weak backscattering and low SNR in the low wind, so there is a large probability of the negative conformity coefficient.

The analysis results indicate that the polarization parameters, typically, the conformity coefficient cannot be used simply for the oil spill detection, and the positive and negative values of the conformity coefficient are not absolutely corresponding to the oil, which are greatly impacted by the noise. The averaged positive SNR of the dark area corresponds to the positive conformity coefficient and the averaged negative SNR corresponds to the negative conformity coefficient. There is no absolute relationship between the incidence angle, the wind speed and the conformity coefficient. The large incidence and the low wind speed have a larger probability for the negative conformity coefficient; while the medium incidence and the high wind speed have a larger probability for positive conformity coefficient.

4.3 *Verification*

To verify the relationship between conformity coefficient and image SNR, another Radarsat-2 data on June 8, 2011 in Norwegian oil-on-water exercise have been used. The image was acquired at 05:59 UTC with an incidence angle of 46.1°–47.3° and a wind speed of 1.6–3.3 m/s. The above analyzed image in Section 4.2 on the same day was acquired after 11.5 h at 17:27 UTC with an incidence angle of 34.5°–36.1° and a wind speed of 1.6–3.3 m/s. The image at 17:27 UTC has averaged noise of –34.5 dB (Migliaccio et al., 2012), with averaged positive SNR for crude oil and emulsion. The image at 05:59UTC has averaged noise of –32 dB (Migliaccio et al., 2012). Figure 13 gives the VV image, SNR, the co-polarization phase and the conformity coefficient of data acquired at 05:59 UTC on June 8, 2011. It could be seen that the backscattering of the VV polarization is mostly lower than noise for emulsified oil, there is no useful information in pdf of the co-polarization phase, and the conformity coefficients are averaged negative.

The two images on June 8, 2011 during the oil spill experiment have nearly the same wind speed, but different incidence angles and SNR levels. The image at 05:59 UTC has the backscattering signal below noise for emulsified oil and negative conformity coefficient. The other image at 17:27 UTC has the backscattering signal above noise for crude oil and positive conformity coefficient. The correspondence of positive/negative SNR and conformity coefficient turns out to be consistent with the results in Section 4.2. The example verifies the correlation between signal to noise level and the conformity coefficient very well.

5 Conclusions and discussion

Radarsat-2 polarimetric SAR data with different incidences, wind speeds, noises and phenomena (oil and look likes) are used to analyze the influence of the observing conditions, the environment parameters and the noises on the polarimetric parameters for the oil slick detection. The following conclusions could be summarized.

(1) The conformity coefficient, Muller parameter $|C|$–B_0 and eigen difference $\lambda_{1,\,\mathrm{nos}}$–$\lambda_{3,\,\mathrm{nos}}$ of the simplified coherency matrix have consistent characterization for the relative magnitude of co-polarization and cross-polarization channels.

(2) The relationship of the conformity and the image signal to noise level has been analyzed for the oil slick, look likes and clean sea. The results indicate that the positive and negative values of conformity coefficient do not absolutely correspond to the oil slick. The conformity coefficient features the signal and noise levels to some extent. When signals are below noise level for the oil slick and look likes, the conformity coefficients are negative; when signals are above noise level for the oil slick and look likes, the conformity coefficients are positive. The clean sea has signal above noise and the positive conformity coefficients. The conformity coefficient tends to be larger under high wind and medium incidence angle than low wind and large incidence angle.

(3) For the dark patches (low wind and biogenic slick, etc.) with SNR below 0, the conformity coefficient, Muller parameters, eigenvalues of the simplified coherency matrix and the co-polarization phase cannot separate them with the oil slick. The low SNR level impedes the detection of the oil slick. For SNR above 0, the oil slick, look likes (low wind and biogenic slick) and clean sea all have the positive conformity coefficient (SAR data at 17:27 UTC on June 8, 2011, for example). The oil slick has the smallest conformity coefficient, the look likes the second, and the clean sea the largest value. So it is possible to discriminate them with the thresholds, while SAR imaging conditions have to be con-

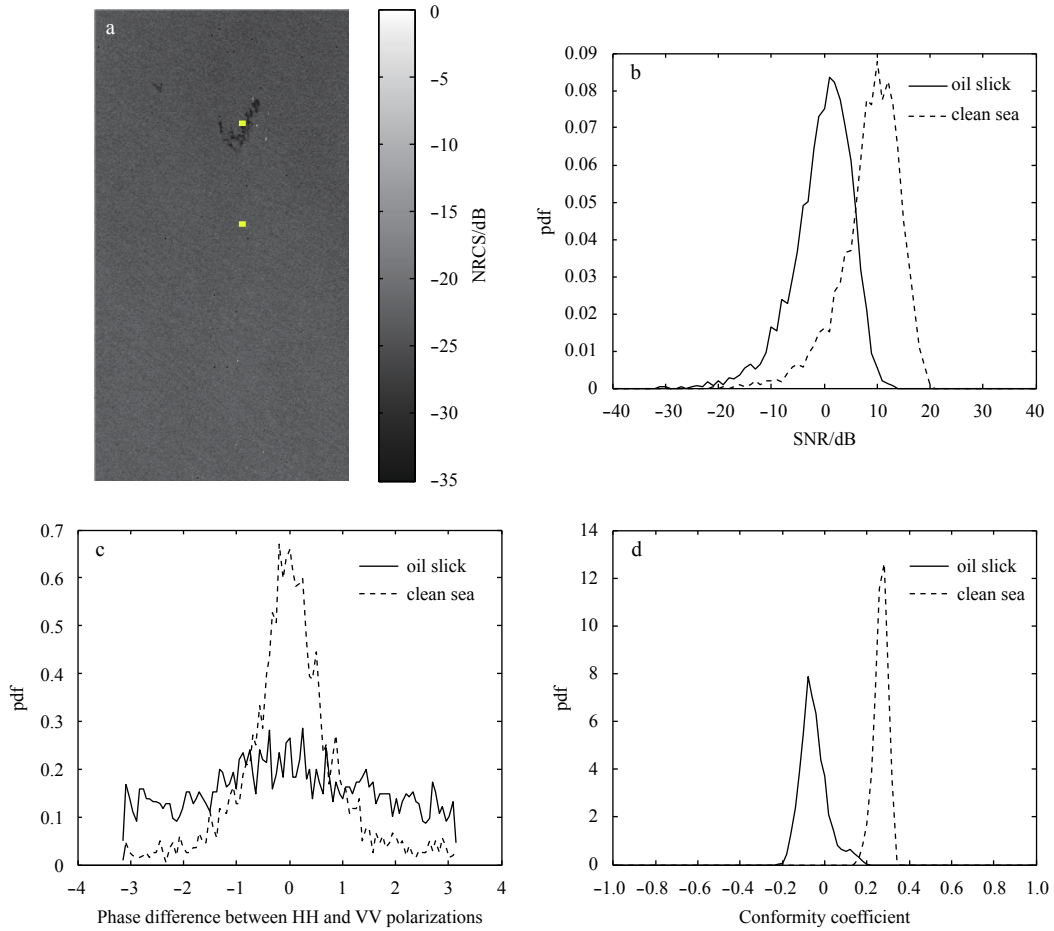

Fig. 13. SAR data at 05:59 UTC on June 8, 2011. VV images (a), SNR pdf (b), co-polarization phase difference pdf (c) and conformity coefficient pdf (d).

sidered. The high SNR level helps to identify the oil slick and excludes the look likes to some extent.

(4) The oil slick detection using the polarimetric SAR data must take the observing conditions, the environmental parameters and the image noises, especially, into account. Only when the signal is above noise for the dark area, the polarimetric parameters can be applied for the oil slick identification. Neither convincible nor stable polarimetric features could be achieved for the oil slick detection once SAR data are involved with the signal below noise.

The conformity coefficient, the Muller parameter $|C|$–B_0 and eigen difference $\lambda_{1,\,\mathrm{nos}}$–$\lambda_{3,\,\mathrm{nos}}$ of the simplified coherency matrix, representing the relative magnitude of co-polarization and cross-polarization channels, have been compared for the oil slick detection, and the typical conformity coefficient has been analyzed for the influence of the observing conditions, the environment parameters and the noises. There are more polarimetric parameters to be analyzed for the influence. As to the SAR imaging incidence and the wind speed, the qualitative analysis in the paper is made to give a probability for their impacts on the polarimetric parameter for the oil detection. More detailed and quantitative analysis should be made. The relationship between the signal to noise level and the conformity coefficient in the paper has been concluded based on eight Radarsat–2 data. More multi-polarization data should be involved in the further work.

References

Allain S, FerroFamil L, Potier E. 2005. New eigenvalue-based parameters for natural media characterization. In: Proc. Of the POLinSAR 2005 Workshop. Frascati, Italy: European Space Agency, 586

Buono A, Nunziata F, Migliaccio M, et al. 2016. Polarimetric analysis of compact-polarimetry SAR architectures for sea oil slick observation. IEEE Transactions on Geoscience and Remote Sensing, 54(10): 5862–5874, doi: 10.1109/TGRS.2016.2574561

Cloud S R. 1985. Radar target decomposition theorems. Institute of Electrical Engineering and Electronic Letters, 21(1): 22–24

Dubois-Fernandez P, Freeman A, Truong-Loi M L. 2008. Soil moisture estimation from compact polarimetry—A viable alternative for SMAP. In: Microwave Remote Sensing for Land Hydrology Workshop. Oxnard, CA: Int. of Electr. And Electron. Eng.

Guissard A. 1994. Mueller and Kennaugh matrices in radar polarimetry. IEEE Transactions on Geoscience and Remote Sensing, 32(3): 590–597, doi: 10.1109/36.297977

Li X F, Li C Y, Yang Z Z, et al. 2013. SAR imaging of ocean surface oil seep trajectories induced by near inertial oscillation. Remote Sensing of Environment, 130: 182–187, doi: 10.1016/j.rse.2012.11.019

Li X, Nunziata F, Garcia O. 2017. Oil spill detection from single- and multipolarization SAR imagery. In: Liang Shunlin, ed. Comprehensive Remote Sensing. Amsterdam: Elsevier, 231–248

Liu Peng, Li Xiaofeng, Qu J J, et al. 2011. Oil spill detection with fully polarimetric UAVSAR data. Marine Pollution Bulletin, 62(12): 2611–2618, doi: 10.1016/j.marpolbul.2011.09.036

Migliaccio M, Nunziata F, Gambardella A. 2009. On the co-polarized

phase difference for oil spill observation. International Journal of Remote Sensing, 30(6): 1587–1602, doi: 10.1080/01431160802520741

Migliaccio M, Nunziata F, Brown C E, et al. 2012. Polarimetric synthetic aperture radar utilized to track oil spills. EOS Transactions American Geophysical Union, 93(16): 161–162, doi: 10.1029/2012EO160001

Migliaccio M, Nunziata F, Montuori A, et al. 2011. A multifrequency polarimetric SAR processing chain to observe oil fields in the Gulf of Mexico. IEEE Transactions on Geoscience and Remote Sensing, 49(12): 4729–4737, doi: 10.1109/TGRS.2011.2158828

Minchew B, Jones C E, Holt B. 2012. Polarimetric analysis of backscatter from the deepwater horizon oil spill using L-band synthetic aperture radar. IEEE Transactions on Geoscience and Remote Sensing, 50(10): 3812–3830, doi: 10.1109/TGRS.2012.2185804

Nghiem S V, Yueh S H, Kwok R, et al. 1992. Symmetry properties in polarimetric remote sensing. Radio Science, 27(5): 693–711, doi: 10.1029/92RS01230

Nunziata F, Gambardella A, Migliaccio M. 2008. On the Mueller scattering matrix for SAR sea oil slick observation. IEEE Geoscience and Remote Sensing Letters, 5(4): 691–695, doi: 10.1109/LGRS.2008.2003127

Nunziata F, Gambardella A, Migliaccio M. 2012. A unitary Mueller-based view of polarimetric SAR oil slick observation. International Journal of Remote Sensing, 33(20): 6403–6425, doi: 10.1080/01431161.2012.687474

Nunziata F, Gambardella A, Migliaccio M. 2013. On the degree of polarization for SAR sea oil slick observation. ISPRS Journal of Photogrammetry and Remote Sensing, 78: 41–49, doi: 10.1016/j.isprsjprs.2012.12.007

Nunziata F, Migliaccio M, Li Xiaofeng. 2015. Sea oil slick observation using hybrid-polarity SAR architecture. IEEE Journal of Oceanic Engineering, 40(2): 426–440, doi: 10.1109/JOE.2014.2329424

Schuler D L, Lee J S, Hoppel K W. 1993. Polarimetric SAR image signatures of the ocean and Gulf Stream features. IEEE Transactions on Geoscience and Remote Sensing, 31(6): 1210–1221, doi: 10.1109/36.317442

Skrunes S, Brekke C, Eltoft T. 2014. Characterization of marine surface slicks by Radarsat-2 multipolarization features. IEEE Transactions on Geoscience and Remote Sensing, 52(9): 5302–5319, doi: 10.1109/TGRS.2013.2287916

Song Dongmei, Ding Yaxiong, Li Xiaofeng, et al. 2017. Ocean oil spill classification with RADARSAT-2 SAR based on an optimized wavelet neural network. Remote Sensing, 9(8): 799, doi: 10.3390/rs9080799

Ulaby F T, Sarabandi K, Nashashibi A. 1992. Statistical properties of the Mueller matrix of distributed targets. IEE Proceedings F - Radar and Signal Processing, 139(2): 136–146, doi: 10.1049/ip-f-2.1992.0017

Van Zyl J. 1989. Unsupervised classification of scattering behavior using radar polarimetry data. IEEE Transactions on Geoscience and Remote Sensing, 27(1): 36–45, doi: 10.1109/36.20273

Van Zyl J, Papas C, Elachi C. 1987. On the optimum polarizations of incoherently reflected waves. IEEE Transactions on Antennas and Propagation, 35(7): 818–825, doi: 10.1109/TAP.1987.1144175

Velotto D, Migliaccio M, Nunziata F, et al. 2011. Dual-polarized TerraSAR-X data for oil-spill observation. IEEE Transactions on Geoscience and Remote Sensing, 49(12): 4751–4762, doi: 10.1109/TGRS.2011.2162960

Wang Chen, Zhao Chaofang, Zeng Kan, et al. 2015. Analysis of scattering mechanisms over sea oil slicks based on eigenvalues of simplified coherence matrix. Journal of Applied Remote Sensing, 2015: 095974

Zhang Biao, Perrie W, Li Xiaofeng. 2011. Mapping sea surface oil slicks using RADARSAT-2 quad-polarization SAR image. Geophysical Research Letters, 38(10): L10602